

Evaporation Residue Production in Complete and Incomplete Fusion Reactions of ^{20}Ne with ^{197}Au and ^{165}Ho at $E = 14.9 \times \text{AMeV}$

Fritz Peter Heßberger^{1,2,*}

¹GSI - Helmholtzzentrum für Schwerionenforschung GmbH, Planckstraße 1, 64291 Darmstadt, Germany

²Helmholtz Institut Mainz, Staudingerweg 18, 55128 Mainz, Germany

Version: April, 27, 2022

Abstract

Velocity distributions of heavy residues ($A_{res} > A_{tar}$), produced in irradiations of ^{197}Au and ^{165}Ho with ^{20}Ne at bombarding energies of $E = 208 \text{ MeV}$, have been measured at the velocity filter SHIP. While for the products from $^{20}\text{Ne} + ^{165}\text{Ho}$ just a mean value of $v/v_{CN} = 0.91 \pm 0.01$ was obtained, individual residues, attributed to isotopes of astatine and polonium with mass numbers ranging from $A = 195$ to $A = 203$ could be identified by means of α spectroscopy in the bombardments of ^{197}Au . A linear increase of the mean velocity from $v/v_{CN} \approx 0.85$ to $v/v_{CN} \approx 0.93$ with decreasing residue mass was observed. This effect was attributed to an increasing contribution of pre-equilibrium particle emission to the production of heavy residues. A quantitative estimation resulted in a 90% contribution of pre-equilibrium processes to the production of astatine isotopes, and a 50% contribution to the polonium isotopes.

1. Introduction

At bombarding energies well above the fusion barrier, in competition to complete fusion, processes arise that are characterized by forming heavy composite nuclei close to the sum of the masses and nuclear charges of projectile and target, but having linear momenta smaller than those of the compound nuclei (CN), having $p_{CN} = p_{proj}$. Since a connection between the missing mass and the missing linear momentum is evident, such processes may be called 'incomplete fusion'. In principle, two scenarios are conceivable: firstly, a break-up of the projectile in the vicinity of the target nucleus, fusion of the latter one with one fragment, while the other one leaves the reaction zone without further interaction, as proposed in [1, 2], or, secondly, emission of particles from the overlap region of the interacting nuclei in a very early stage of the reaction (see e.g. [3, 4]). In both cases no or only little interaction of the escaping particles with the target nucleus has occurred, so their velocity is close to that of the projectiles and their angular distributions peak around the beam direction. Since they appear to be emitted before a complete amalgamation of projectiles and target nuclei has occurred, i.e. thermal equilibrium was reached, they may be denoted as 'pre-equilibrium' particles. In this sense 'incomplete fusion' is accompanied by the emission of 'pre-equilibrium' particles, while vice versa the occurrence of 'pre-equilibrium' particles is no unambiguous indication for incomplete fusion, however: the second projectile fragment may leave after, e.g. donating or accepting a few nucleons, and also projectile and target nuclei may recombine again, without having formed a 'compound' nucleus.

In this sense we will distinguish here three cases, despite the fact, that naming may be treated in a different way in literature.

- 'incomplete fusion': fusion-like processes without full momentum transfer, i.e. 'evaporation' of light particles with velocities close to the projectile velocities, different to light particles emitted from a fully equilibrated composite nucleus ('compound nucleus') having a 'thermal' energy spectrum.
- 'fusion after projectile break-up': break-up of the projectile in vicinity of the target nucleus; fusion of one projectile fragment with the target nucleus, while the other one escapes the reaction zone without further interaction.
- 'transfer reactions': exchange of a 'couple' of nucleons between projectile and target nucleus at contact, followed by recombination of both reaction partners.

In recent experiments we have investigated the production of heavy residues in bombardments of ^{197}Au (at 114, 172 and 228 MeV) and ^{208}Pb (at 172, 228 and 298 MeV) with ^{20}Ne [5, 6, 7, 8]. Significant contributions of incomplete fusion to the heavy residue production, indicated by a shift of the mean velocity of the residues to values $v_m/v_{CN} \approx 0.90$ -0.95, was observed already at a bombarding energy of 172 MeV, which were interpreted as due to 'incomplete fusion'. In addition in reactions $^{20}\text{Ne} + ^{208}\text{Pb}$ a 'slow' residue component at $v_{m,slow}/v_{CN} \approx (0.40$ -0.60) was observed, which appeared to decrease significantly towards the highest bombarding energy, in accordance with the model proposed in [2], while the mean velocity of the 'fast' component was still decreasing.

*E-mail: f.p.hessberger@gsi.de

As a completion of these measurements we here want to present the results for $^{20}\text{Ne} + ^{197}\text{Au}$ at $E = 208$ bombarding energy.

2. Experimental set-up

The experiments essentially were performed with beams of ^{20}Ne ($E = 11.4 \times A$ MeV (228 MeV) and $14.9 \times A$ MeV (298 MeV)) from the UNILAC accelerator at GSI, Darmstadt. For light particle measurements also short irradiations at $E = 5.9$ AMeV (118 MeV) and 8.6 AMeV (172 MeV) were performed. The ^{20}Ne beam had a repetition rate of 50 Hz and a duty factor of 23%, i.e. each pulse of 4.6 ms duration was followed by a pause of 15.4 ms ('macro pulses'). The ^{197}Au targets were thin rolled foils of $\approx 180 \mu\text{g}/\text{cm}^2$, while the ^{165}Ho targets were produced by evaporating the material ($\approx 60 \mu\text{g}/\text{cm}^2$) on a carbon backing of $\approx 30 \mu\text{g}/\text{cm}^2$ or were rolled foils of $\approx 600 \mu\text{g}/\text{cm}^2$. Typical beam intensities of 30-50 pA were used in the irradiations of ^{197}Au and 5-10 pA in the ^{165}Ho irradiations.

The evaporation residues (ER) recoiled from the targets nearly unretarded. They passed a thin ($\approx 15 \mu\text{g}/\text{cm}^2$) carbon foil, which was placed 8 cm downstream the target position to equilibrate the ionic charge distributions of the evaporation residues. They were separated by the velocity filter SHIP [9] and were focussed to a detector system. Since in the current experiments a broad angular distribution was expected for the evaporation residues, the angular acceptance of SHIP was increased from 1.5° to 3.5° by placing the targets 80 cm closer to the entrance of the first quadrupole triplet. From model calculations [10, 11, 12] an enhancement of the efficiency by a factor 2-3 could be expected.

The detection system consisted of two transmission detectors [13], 447 mm apart, that were used for the 'fine' velocity measurements of the evaporation residues, and two silicon detector arrangements, placed closely one after the other. The first one ('stop detector'), in which the evaporation residues were implanted, was a passivated ion implanted silicon detector of $60 \times 24 \text{ mm}^2$ and had an effective thickness of $300 \mu\text{m}$. It was subdivided into ten strips, each of $6 \times 24 \text{ mm}^2$. Besides registration of the incoming evaporation residues, the 'stop detector' was used to measure the α -decay energies of the implanted nuclei. The energy resolution of the individual strips varied between (15-19) keV (FWHM) for α particles in the range (5-8) MeV.

The second detector ('light particle detector' (LPD)), an array of $3 \times (24 \times 24) \text{ mm}^2$ passivated ion implanted silicon chips of $300 \mu\text{m}$ thicknesses, was used to detect high energetic light particles that passed SHIP and also the 'stop detector' and could prevent evaporation residues or α decays due to their energy loss in the 'stop detector'. The combined system also allowed for light particle identification due to $\Delta E_{\text{stop}} - E_{\text{LPD}}$ or $\Delta E_{\text{stop}} - \Delta E_{\text{LPD}}$ measurements.

For each registered event additionally the absolute time as well as the time within the 'macro pulse' were registered with continuously running clocks. These informations were used in the off-line analysis to distinguish between events occurring during the beam bursts and those occurring within the pause and also to measure decay curves after the end of each irradiation. The beam current was measured at the beam stop of SHIP. It was digitized and also registered.

The signals of the individual detectors were processed by conventional NIM/CAMAC modules and stored on tape event-by-event. Data acquisition and on-line analysis was performed with a VAX86 computer using the GOOSY system [14], while off-line analysis was performed at an IBM3090-60J computer at GSI using the SATAN system [15].

3. Efficiency considerations

To convert the measured particle rates into cross sections we have to consider the efficiency of our set-up, which can be defined as the product of the SHIP transmission and the detection efficiency. The former is critically dependent on the angular distribution of the evaporation residues. Since for the products in question very small transmission values of one per cent are expected [10, 11], already small variations, caused e.g. by deviation of the energy and angular distributions of the evaporated particles from those used in the model calculations, may lead to significant changes in the transmission values. As another consequence it follows that the SHIP transmission also depends on the evaporation channel. So, principally, a check of the calculated transmission values requires a complete set of independently measured cross sections for the same or a similar reaction, which is hardly feasible for the systems considered here. Thus we contented ourselves with a comparison of the evaporation residue cross section for $^{20}\text{Ne} + ^{165}\text{Ho}$ at $E = 290$ MeV, where a value of $\sigma = 450$ mb is reported [16]. (Here σ is taken as the sum of evaporation residues from complete fusion and incomplete processes where one preequilibrium proton or one preequilibrium α -particle is emitted.) Using this value we obtain a SHIP transmission of $\epsilon \approx 0.034$ averaged over all evaporation channels. To compare this experimental value with model calculations we used the fusion - evaporation codes HIVAP [17] as well as ALICE [18] to calculate the isotopic distribution of the residues, allowing as well emission of neutrons, protons and α particles as the emission of neutrons and protons only. The sense of the latter procedure was to estimate the relative

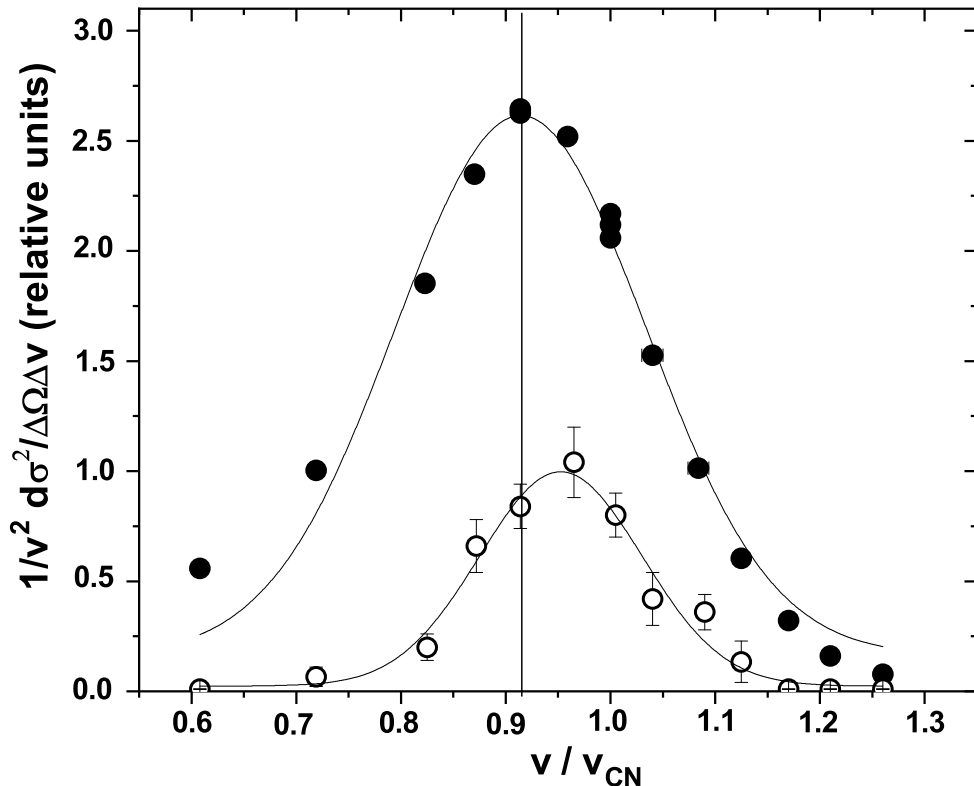


Fig. 1: velocity distributions for evaporation residues from $^{20}\text{Ne} + ^{165}\text{Ho}$ at $E = 298$ MeV. Full dots: all evaporation residues; open circles: ^{170}Os

contributions of $\alpha\gamma\text{pzn}$ - deexcitation channels and γpzn - deexcitation channels to specific residues. The cross sections for the individual residues were weighted with their calculated transmission values and integrated. As a result an averaged calculated transmission of $\epsilon = 0.027$ was obtained. We are aware of the fact that preequilibrium emission may significantly change the isotopic distribution of the residues as well as the SHIP transmission for specific deexcitation channels. So the fair agreement between the experimental and calculated transmission may be somewhat fortitious.

For the somewhat heavier system $^{20}\text{Ne} + ^{197}\text{Au}$ we obtain from our calculations transmission values of $\epsilon \approx (0.02-0.03)$ for γpzn - channels and $\epsilon \approx (0.005-0.001)$ for $\alpha\gamma\text{pzn}$ - channels.

Conservatively we do not claim the cross section values more reliable than within a factor of three.

4. Experimental results

4.1 Velocity distributions

Since SHIP is a Wien type velocity filter, velocity distributions of evaporation residues can be measured just by changing the E/B - ratio (see ref.[5] for details). A drawback of this method, however, is that the velocity distribution of the evaporation residues is folded with the (velocity dependent) transmission of SHIP. As a consequence, the mean velocity of the detected residues in general will be slightly different from the preset velocity defined by the E/B - ratio. To overcome this problem we measured the velocities explicitly using the time-of-flight system mentioned above. The velocities obtained were corrected for the energy loss in the carbon foil ($\approx 30 \mu\text{g}/\text{cm}^2$) of the first transmission detector using the

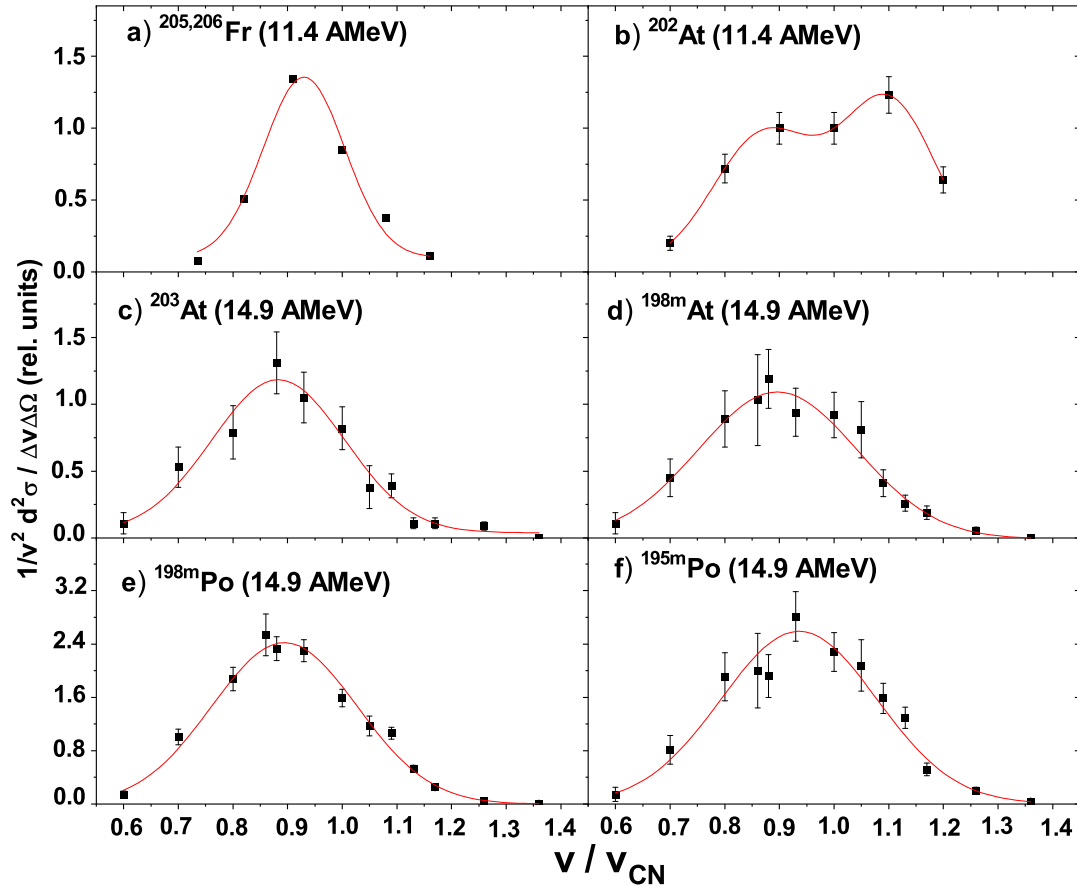


Fig. 2: velocity distributions for evaporation residues from $^{20}\text{Ne} + ^{197}\text{Au}$

energy loss table of ref. [19]. The deviation between the preset velocity $v_{E/B}$ and the measured velocity v_{TOF} was found to be $|1 - v_{E/B}/v_{TOF}| \leq 0.03$.

The velocity distributions measured for $^{20}\text{Ne} + ^{165}\text{Ho}$ are shown in fig. 1. In this reaction only one α emitter, ^{170}Os (open circles) which represents the p14n - channel of the compound nucleus ^{185}Ir was registered with an intensity high enough to evaluate a velocity distribution. Its production rate was only a fraction of 2.4×10^{-4} of the total evaporation residue production rate.

The full dots in fig. 1 represent the distribution for the evaporation residues, registered by ion counting. While the distribution of ^{170}Os peaks at $v/v_{CN} = 0.95 \pm 0.01$, that for the evaporation residues peaks at a significantly lower value of $v/v_{CN} = 0.91 \pm 0.01$. The difference can be interpreted due to a different number of particles emitted predominantly in forward direction, denoted in the following as 'preequilibrium particles' despite of possibly originating from different nuclear processes. For ^{170}Os the emission of one preequilibrium particle (proton or neutron) on the average is suggested. For the evaporation residues, as they represent the sum over all deexcitation channels, weighted by the SHIP transmission (see sect. 3) the situation is more complicated. As the bulk of the mass distribution is represented by isotopes which are no α emitters, most probably those with $Z < 76$ and $N > 94$, the value of v_m/v_{CN} just represents a mean value, that does not allow for a definite conclusion about the mass or the number of emitted preequilibrium particles in each process leading to an evaporation residue with a definite A_{ER} and Z_{ER} . It just may be concluded that it represents the bulk of residues where up to four mass units were taken away by preequilibrium particles.

A significant deviation from the shape of a single Gaussian, however, is evident for evaporation residues at $v_m/v_{CN} < 0.7$. This behavior is interpreted as due to contributions of incomplete fusion fractions with mass transfer $A_{tr} < 16$, or, vice versa, the removal of four units of mass by preequilibrium emission, in accordance with the results in ref. [16].

Typical examples of velocity distributions for evaporation residues from irradiations of ^{197}Au with ^{20}Ne are shown in figs. 2c-f. For comparison we present examples from the 11.4 AMeV - measurement in a previous experiment [5] in figs. 2a, 2b. Different to ^{202}At produced at 11.4 AMeV (fig. 2b) for none of the produced isotopes an enhanced intensity at $v/v_{CN} > 1$ is clearly indicated at 14.9 AMeV, i.e. contributions from emission of thermal α particles to the evaporation residue production must be regarded as negligible.

Instead we observe, similar to $^{205,206}\text{Fr}$ produced at 11.4 AMeV rather symmetric distributions with maxima shifted to $v_m/v_{CN} = (0.86-0.94)$.

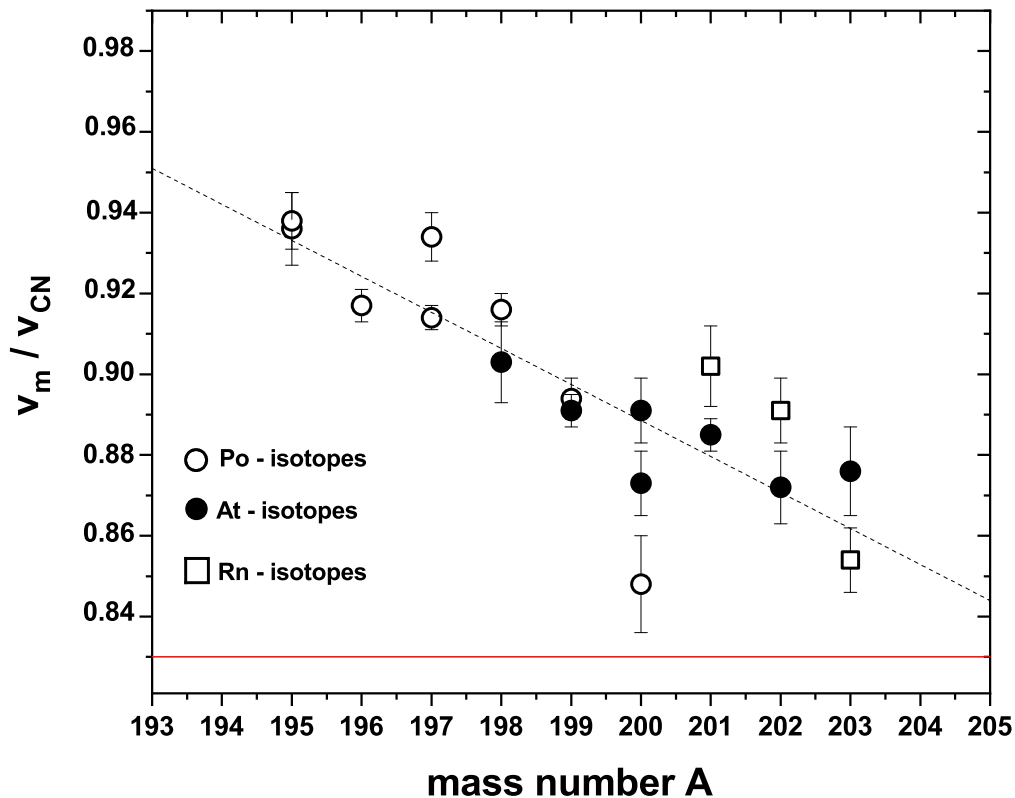


Fig. 3: mean velocities of evaporation residues from $^{20}\text{Ne} + ^{197}\text{Au}$ at $E = 298$ MeV; open circles = polonium isotopes, full circles = astatine isotopes, open squares = radon isotopes

The positions of the maxima were found to depend significantly from the residues mass A_{ER} : we unambiguously observe the highest mean velocities for the lightest residues. A dependence of v_m/v_{CN} from the atomic number Z_{ER} (fig.3) of the residues is not indicated. The mass dependence v_m/v_{CN} can be understood as a consequence of an interplay between emission of 'thermal' and preequilibrium particles during deexcitation. Since the velocities (and thus the energies) of the preequilibrium particles are higher than those of thermal particles, they will cool down the excited nucleus more effective than thermal ones. Preequilibrium emission thus will lead to heavier residues. Since the angular distributions of preequilibrium particles is peaked in forward direction, while thermal particles are emitted essentially isotropic, a net shift to lower mean velocities will occur. The magnitude of the shift will be governed by the multiplicity, mass and energy of the preequilibrium particles emitted in the process leading to a specific residue. The widths of the distributions (FWHM) vary between 24% and 34% of v_{CN} . An unambiguous dependence on the residue masses, however, is not indicated.

4.2 Cross sections

Cross sections can be deduced from the intensity of the α lines according to the efficiency considerations in sect. 2.

From the α spectra we obtain total cross sections of $\sigma(\text{At}) = 825 \pm 63 \mu\text{b}$ for the At-isotopes. For the Po - isotopes we observe a comparable cross-section of $\sigma(\text{Po}) = 572 \pm 20 \mu\text{b}$, while for the Rn - isotopes a contribution of only about $10 \mu\text{b}$ is obtained. For the total amount of evaporation residues, registered by ion counting, we obtain a value $\sigma(\text{ER}) = 2.9 \pm 0.1$ mb. The α emitters thus contribute to about 48 % of the total residue cross-section. The cross-sections for the individual residues, identified by their α decay, are displayed in fig. 4 in comparison with model calculations (see sect. 5.2). For astatine we observe the maximum cross-section at about $A = 200$, while for polonium the values appear almost constant in the region $A = 196$ and $A = 200$. The bulk of the residues ($\approx 52\%$) seems to be represented by Po - isotopes

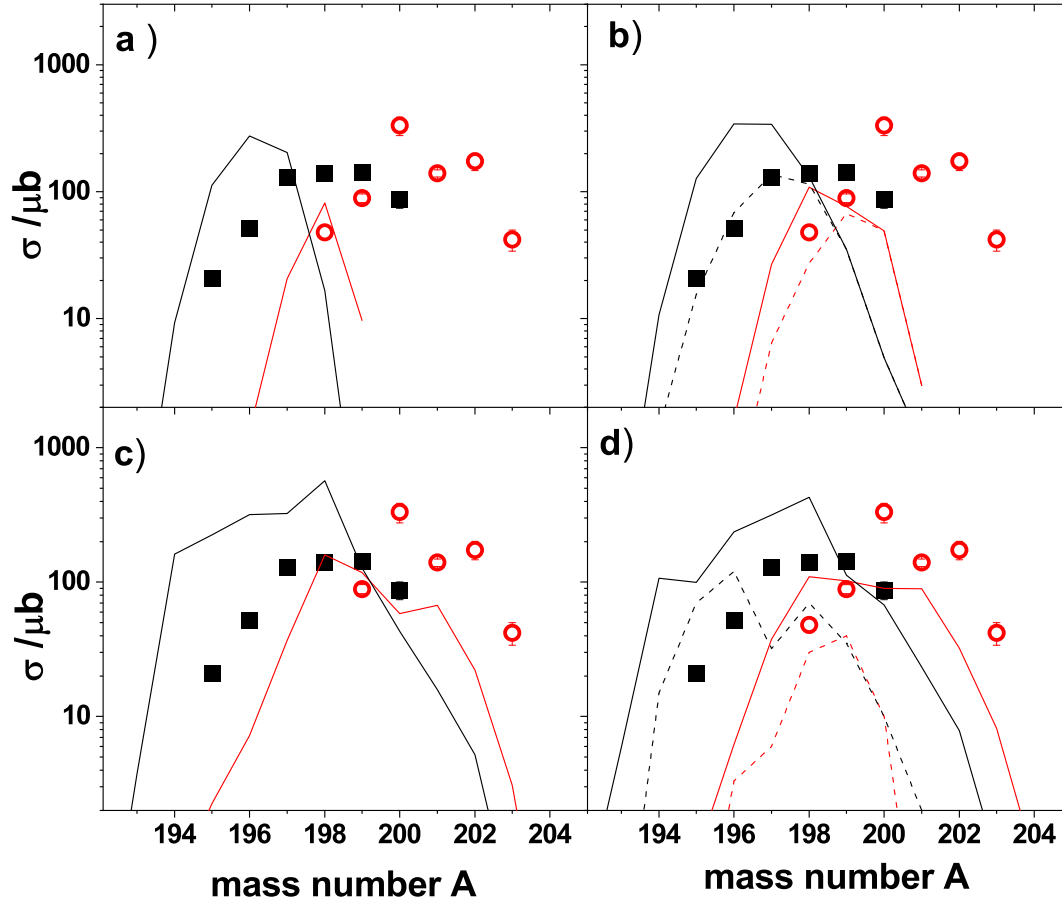


Fig. 4: evaporation residue cross sections for $^{20}\text{Ne} + ^{197}\text{Au}$ at $E = 298$ MeV, full squares: polonium isotopes, open circles: astatine isotopes. The lines are the result of calculations for Po- isotopes (black) and At- isotopes (red); a) full lines: HIVAP calculations, complete fusion; b) full lines: sum rule model + HIVAP, complete and incomplete fusion; dashed lines: sum rule model + HIVAP, only incomplete fusion; c) full lines: ALICE calculations; d) full lines: ALICE + standard hybrid model, dashed lines: sum rule model + ALICE.

with masses $A > 200$ and nuclei with atomic numbers $Z < 84$, which have α branches $b_\alpha < 0.05$ and are not identified unambiguously in our experiment. The shift by about two mass units from $Z = 85$ to $Z = 84$ may indicate that the polonium isotopes are produced to a higher extent by emission of preequilibrium α particles from the composite nucleus.

4.3 Light particle measurements

Due to their high magnetic and electric rigidity high energetic light particles (protons, α particles etc.) are only weakly deflected by SHIP; thus they can pass the separator and be detected. For this purpose two Si-detectors, forming a 'telescope' were mounted in the focal plane of SHIP. Despite the small solid angle ($\Omega \approx 1.2 \times 10^{-6}$) due to their high production cross sections notable amounts of such particles can be registered in relatively short irradiation times. To ensure that indeed the particles stem from reactions with the target material, such measurements were performed only with the gold targets, as they did not have carbon backings. Also the carbon converter foil was removed. The measurements were performed at four bombarding energies $E_{lab} = 118, 172, 228$ and 298 MeV. A two-dimensional plot of energies or respectively energy losses ΔE_1 ('stop detector') versus ΔE_2 ('light particle detector') at the bombarding energy of $E_p = 298$ MeV is shown in Fig. 5. Four groups of particles could be identified: a) $Z=1$ - particles, protons or deuterons (1), b) $Z=2$ - particles, α particles or ^3He nuclei (2), c) $Z=3$ - particles, Li - nuclei (3), and d) $Z=4$ - particles, Be-nuclei (4). This arrangement allowed for detection of, e.g. α - particles in the range $E \approx 22\text{--}32$ MeV. α - particles of lower energy ($E < 23$ MeV) are fully absorbed in the stop detector and thus are not visible in the $\Delta E_1 - \Delta E_2$ plane. At higher particle energies ΔE_1 decreases with increasing energy while the energy ΔE_2 measured in the LPD increases (upper branch)

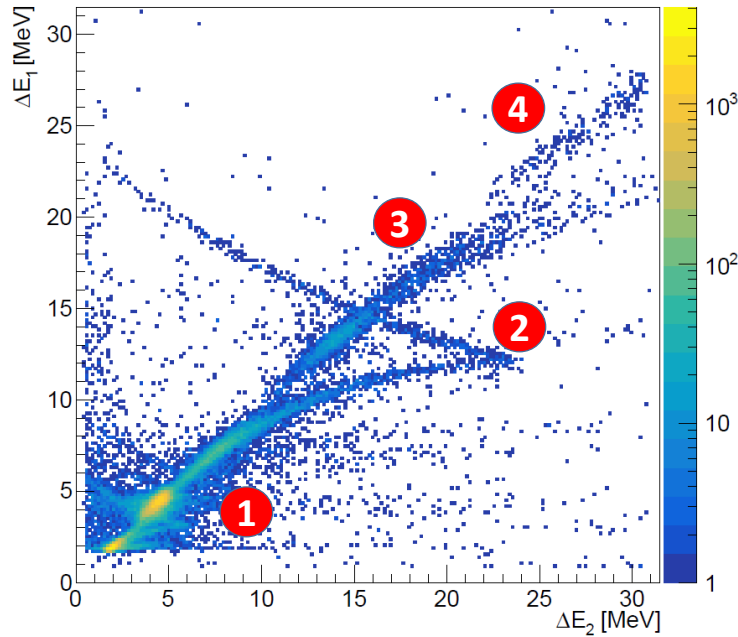


Fig. 5: Light particle spectra measured with the detector telescope ('stop detector' + 'light particle detector' (LPD)) behind SHIP.

until a value $\Delta E_2 \approx 25$ MeV is reached. Particles of higher energies can punch through the LPD, and we observe both, decreasing ΔE_1 and decreasing ΔE_2 values. The bulk of the distribution was found at $\Delta E_1 \approx \Delta E_2 \approx 7.5$ MeV, corresponding to a total of $E = 55$ MeV, reconstructed using the energy loss of α particles in silicon according to [20]. The energy distributions of the α particles could be divided into two components: a) one of $E \approx 30$ MeV, only varying slightly with the beam energy, which was ascribed to 'thermal - evaporation' α particles, and b) a component with energies suggesting velocities close to the projectile velocity (shown in fig. 6), which was ascribed to 'preequilibrium' α particles.

It should be remarked, that at the specific beam energies neither the energy nor the intensity of the preequilibrium α - particles depended on a specific velocity setting of SHIP, which means, that these particles past SHIP nearly undeflected.

5. Discussion

5.1 Incomplete Fusion

As it was already discussed in sect. 4.1, the velocity distributions for the different residues reflect a competition between emission of only thermal particles and, in addition, also preequilibrium particles during the deexcitation of the hot composite nuclei.

Thus it seems meaningful to decompose the measured velocity distributions into a 'complete' fusion (emission of only thermal particles) and an 'incomplete' fusion (emission of preequilibrium particles in addition to thermal particles) fraction. The velocity distribution for complete fusion was estimated by model calculations [10, 11], taking into account emission of thermal nucleons (protons and neutrons) only. To determine both fractions we fitted the measured velocity distributions each by two gaussians. Peak positions and FWHM for that representing complete fusion were taken from the model calculations. Strictly, one would have also to respect emission of thermal α particles, which, however leads to strong components in the distributions for $v/v_{CN} > 1$. Experimentally such contributions are not evident for $^{20}\text{Ne} + ^{197}\text{Au}$ at $E = 14.9$ AMeV (see figs. 2c-2f). Fits including also velocity distributions expected for α - channels in the complete fusion fraction resulted in contributions of < 0.01 for the At-isotopes and < 0.05 for the Po-isotopes. Thus contributions from α pyn channels were neglected. The ratio of the peak areas $\gamma = A_{inc}/(A_{inc} + A_{com})$, where A_{inc} , A_{com} denote the areas of the gaussians attributed to incomplete and complete fusion, respectively, was taken as a measure for the completeness of the fusion leading to the production of the specified evaporation residue. The results are shown in fig. 7. A significantly different behavior for the At ($Z=85$) and Po ($Z=84$) - residues is evident. The 'incomplete fusion'

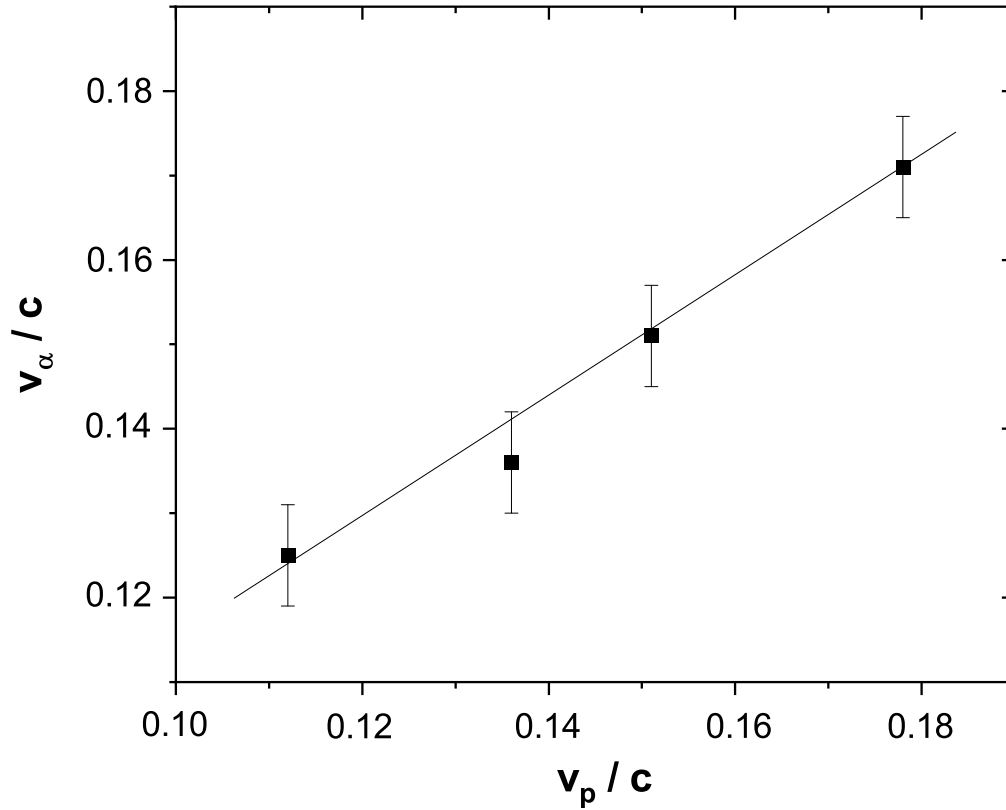


Fig. 6: Mean velocity (v_α) of the 'high energy' α particle component as function of the projectile velocity (v_p)

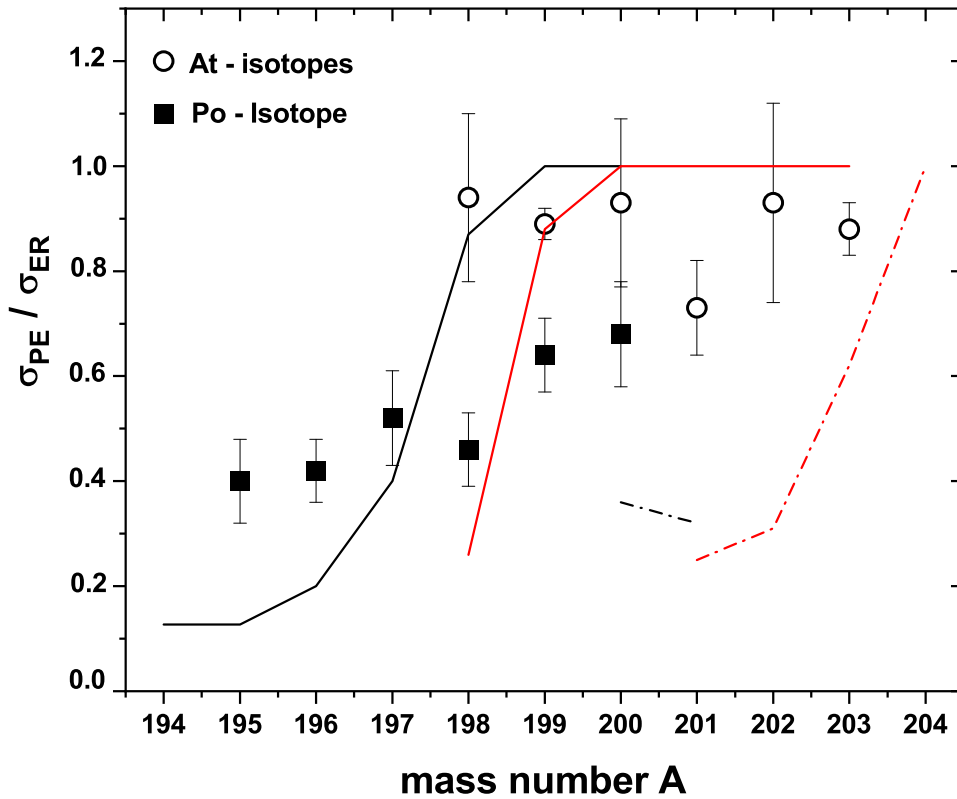


Fig. 7: Fraction of residues from incomplete fusion to total. Open circles: astatine isotopes, full squares: polonium isotopes; full lines: results from calculations using sum rule + HIVAP for polonium (black) and astatine - isotopes (red); dashed dotted lines: results from ALICE + standard hybrid model calculations

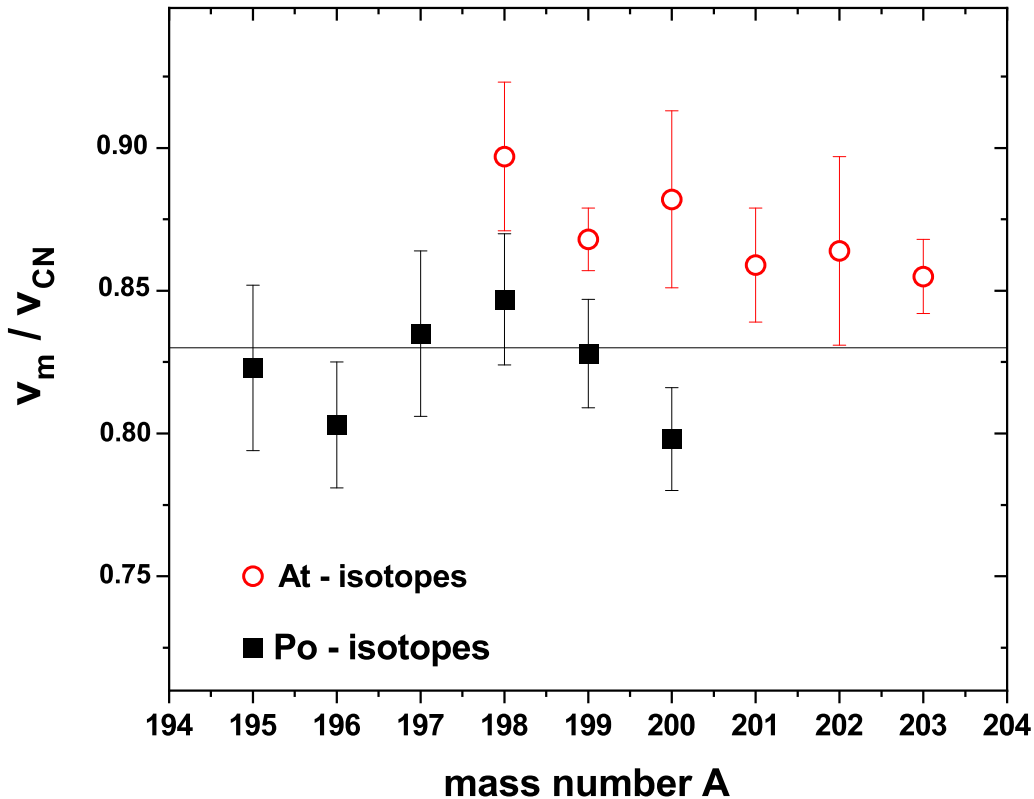


Fig. 8: mean velocities of the incomplete fusion component of evaporation residues from $^{20}\text{Ne} + ^{197}\text{Au}$ at $E = 298$ MeV; open circles: astatine isotopes, full squares: polonium isotopes. The line represents the mean velocity obtained from fusion-fission reactions.

fractions for the At-isotope is constant, typically around 90% of the total, while for the Po-isotopes it is increasing from $\approx 40\%$ to $\approx 70\%$ with increasing residue mass number. Qualitatively this behavior might be understood as due to the influence of different multiplicities and masses of preequilibrium particles. This behavior, however, is not well reproduced by model calculations using either the sum rule model for calculating the reaction cross sections and HIVAP for deexcitation (full lines in fig.7) or ALICE and the standard Hybrid model (dashed-dotted lines in Fig.7). While stable values around $\gamma = 1$ are obtained for $A \geq 199$ (Po - isotopes) and $A \geq 200$ (At - isotopes) and a steep decrease towards lower mass values are obtained from the calculations, stable values of $\gamma \approx 0.90$ for the At-isotopes and a moderate increase of γ with increasing mass number are observed for the Po-isotopes. The ALICE + standard hybrid model calculations (dashed-dotted lines), however, do not reproduce the experimental data at all.

A somewhat different behavior is found for the maxima (or 'mean velocities') of the 'incomplete fusion' component as obtained from the fits and shown in fig. 8. Despite of large error bars and straggling of the data we observe significantly different values for the At- and Po-isotopes, We obtain mean values, averaged over all isotopes observed, of $(v/v_{CN})_{incomp} = 0.87 \pm 0.02$ for the astatine and $(v/v_{CN})_{incomp} = 0.82 \pm 0.02$ for the polonium isotopes. For the At-isotopes further a trend to decreasing mean velocities for increasing masses is indicated. These values indicate that in incomplete fusion processes leading to the production of At-isotopes about (2-3) nucleons are emitted on the average prior to thermal equilibrium, in those leading to Po-isotopes four mass units are carried away on the average (probably predominantly as an α particle) by preequilibrium processes. Thus the Po-isotopes are produced with nearly equal fractions either by incomplete fusion, accompanied by emission of preequilibrium particles, or by complete fusion followed by emission of thermal nucleons, but only to a small extent by emission of thermal α particles during deexcitation. Contrary to the situation at lower bombarding energies [5], where we observed a competition between preequilibrium and thermal α particles, we seemingly here have an 'either - nor' situation, i.e. either a preequilibrium α particle is emitted or no α particle will be emitted during the deexcitation process.

Our experiments indicate higher mean velocities of the evaporation residues than the value obtained from linear momentum transfer measured in fusion-fission reactions [21] assuming the missing momentum is carried away by one or several particles moving in beam direction and with the projectile velocity (see fig. 3). Comparing the results of [21] with the results of the incomplete component for the individual isotopes (see fig. 8), an agreement between fusion - fission results and the velocities for the Po-isotopes is indicated, while those for the At-isotopes the mean velocity is higher. In [5] we compared the intensity

ratio of preequilibrium and thermal α particles measured in [22] and our cross-section ratios for evaporation residue production including preequilibrium emission and solely thermal emission. We found that only a small part of the preequilibrium α particles contributed to the evaporation residue production (compared to thermal ones) and concluded that preequilibrium production was connected to high angular momenta.

This interpretation is in-line with the sum-rule model of Wilczinski et al.[2]; a) break-up of ^{20}Ne into $^{16}\text{O} + ^4\text{He}$ followed by fusion of ^{16}O with ^{197}Au , while the α particle moves on with beam energy and is considered as a 'preequilibrium particle'. This process is limited to a narrow l-window close to the grazing angular momentum, leaving the incomplete compound nucleus ^{213}Fr at a high angular momentum of $\hbar \approx 68$, where its fission barrier is zero, and an excitation energy of $E^* \approx 130$ MeV; so at a bombarding energy of 11.4 AMeV only branches of low l-values can contribute to the evaporation residue production. The same holds for break-up $^{20}\text{Ne} \rightarrow ^{19}\text{F} + \text{p}$ etc.. At $E = 14.9$ AMeV we expect from the sum-rule model about the same angular momentum, but a higher excitation energy of $E^* \approx 180$ MeV; b) in bombardments of ^{208}Pb with ^{20}Ne 'slow' evaporation residues were attributed to (incomplete) fusion after projectile break-up into more symmetric fractions, leading to lower angular momenta of the composite system were observed [7]. This component was present at bombarding energies $E = 8.6$ AMeV and 11.4 AMeV, but not observed at $E = 14.9$ AMeV.

5.2 Mass Distributions

To achieve further insight we compared our measured evaporation residue cross sections with model calculations. In one set of calculations we used the sum-rule model to obtain the reaction cross-section as well as the excitation energies and angular momentum distributions for the products from complete fusion reactions and the different incomplete fusion channels, and used the HIVAP code [17] for deexcitation. Alternatively we used the ALICE code [18]. The results are presented in fig 4.

In figs. 4a, 4b we present the results using the sum-rule model plus HIVAP. According to recent results on 'fission hindrance' (see e.g. [23]) at high excitation energies, the Γ_f - value from HIVAP was scaled by a parameter $\exp((E^* - E_{th}/E_\tau))$. Using $E_{th} = 90$ MeV and $E_\tau = 20$ MeV (we do not stress to much attention to these specific numbers), a reproduction of the residue cross section values by a factor of five was achieved in a narrow region of residue masses. But neither respecting complete fusion alone (fig. 4a), nor including incomplete fusion component (fig. 4b) by summing all contributions from projectile fragments $A_{pf} \leq A_p - 6$ (lighter projectile fragments lead to residues with lower velocities) were able to reproduce the measured mass distributions for both, the At- and the Po-isotopes. The calculated mass distributions are narrower and shifted towards lower masses. Even respecting incomplete fusion, we still fail to reproduce the cross sections for the heaviest masses.

A similar situation is evident for the ALICE - calculations. We get here a broader mass distribution already when respecting only complete fusion (fig. 4c). The inclusion of preequilibrium emission using the hybrid model with standard parameters results in a notable increase of the cross-sections on the heavy mass side, but still underpredicts the experimental data (fig 4d). A similar situation is observed when the results from the sum-rule model calculations are used as input for deexcitation calculations with ALICE (dashed lines in fig. 4d). Here the steep decrease sets in already at lower mass numbers.

It is further evident, that in all types of calculations the cross sections for the lighter polonium isotopes are overestimated in general, while those for the heavier ones are underestimated. For the astatine isotopes they are underestimated in general. Although, in principle, it cannot be excluded, that this behavior is due to an incorrect treatment of the fission barriers, we suppose a higher contribution of incomplete fusion than predicted by the models used here, leading to an enhanced production of heavier residues. It seems, however, questionable that this fraction can be attributed to a higher contribution from fusion after projectile break-up rather than by pre-equilibrium emission, as this reaction type would lead to lighter residues, as shown by both the HIVAP and the ALICE results.

So tentatively we would thus ascribe the enhanced cross sections for the heavier masses to particle emission from the interaction zone in an early stage of the reaction, as described, e.g. in [3, 4], but with higher emission rates and probably with higher multiplicities or higher masses. The angular momentum distribution of composite systems produced in such processes were recently investigated theoretically by Krishan et al. [24]. They found a considerable lowering of the angular momentum compared to complete fusion, e.g. by $20\hbar$ for $^{27}\text{Al} + ^{84}\text{Kr}$ at $E = 20$ AMeV.

Since emission of preequilibrium particles further reduces the excitation energy, the influence of both further could contribute to an enhancement of the stability against prompt fission and thus to enhanced residue cross-sections.

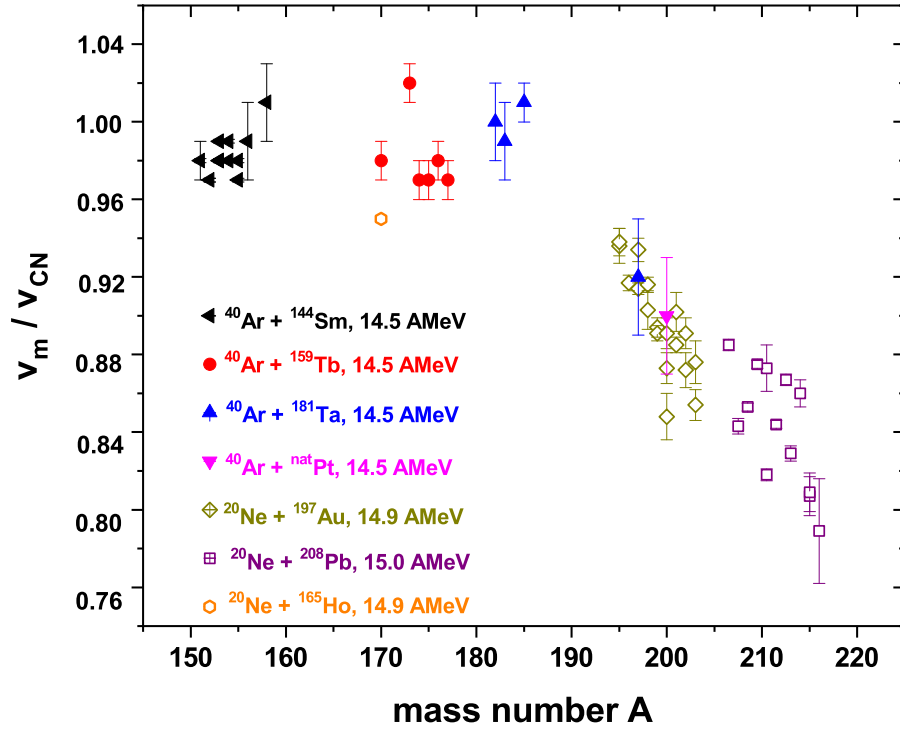


Fig. 9: Mean velocities of evaporation residues from $^{40}\text{Ar} + ^{144}\text{Sm}$, ^{159}Tb , ^{181}Ta , $^{\text{nat}}\text{Pt}$ at $E = 580$ MeV, $^{20}\text{Ne} + ^{165}\text{Ho}$, ^{197}Au at $E = 298$ MeV, $^{20}\text{Ne} + ^{208}\text{Pb}$ at $E = 300$ MeV.

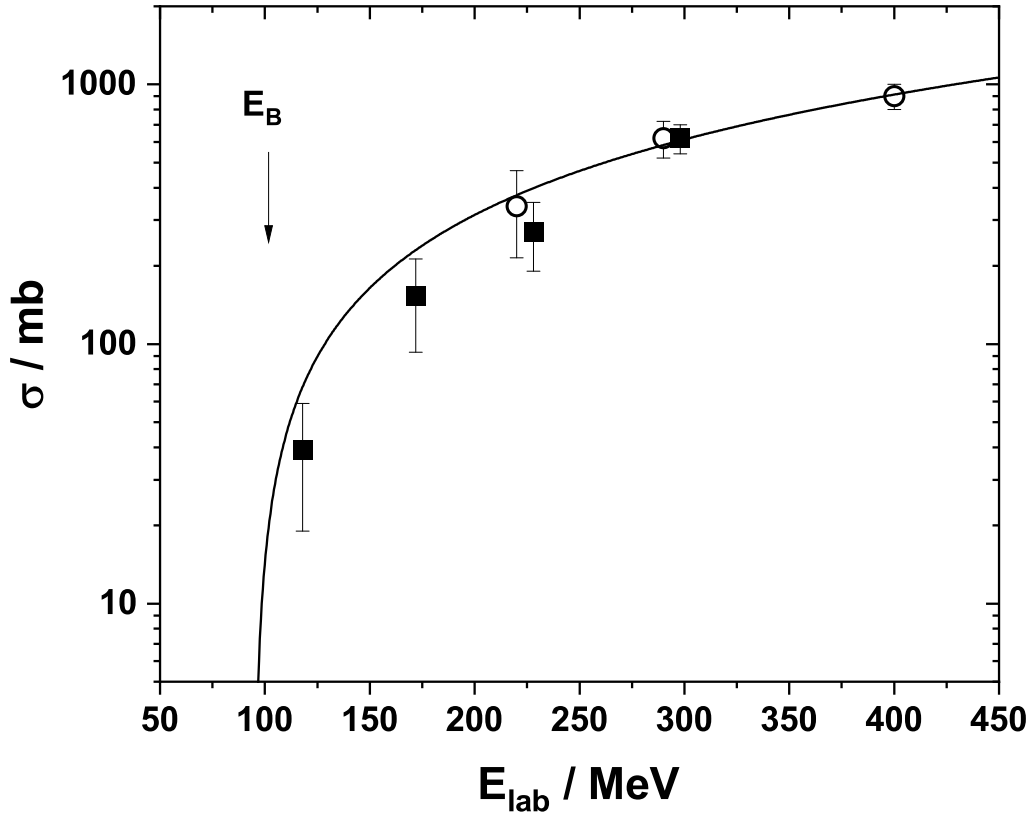


Fig. 10: Intensities of preequilibrium α - particles as a function of the projectile energy E_p . Open circles: data from [22]; full dots: data from this work, normalised to those from [22]. The full line is the result of fitting a straight line the data of [22].

5.3 Velocity Distributions

Here we again want to mention the velocity distributions and give one more comment. In fig. 9 we present a comparison of mean velocities for residues from Ar - induced reactions at $E = 14.5$ AMeV (full symbols) [25] and Ne - induced reactions (open symbols); the circles refer to data from this experiment for $^{20}\text{Ne} + ^{197}\text{Au}$, the hexagon for ^{170}Os from $^{20}\text{Ne} + ^{165}\text{Ho}$, the squares to data from $^{20}\text{Ne} + ^{208}\text{Pb}$ [7] at 15.0 AMeV. Both sets of data refer to similar projectile velocities above the Coulomb barrier.

For $A_{res} < 200$ there is some indication, from the different mean velocities of the residues from the ^{40}Ar - induced reactions and ^{170}Os from $^{20}\text{Ne} + ^{165}\text{Ho}$ that the sum of the masses of the emitted preequilibrium particles on the average is constant for the same projectile velocities irrespective of their masses. Better experimental data to support this evidence are necessary, since such a behavior would be in contradiction to the conclusions of several authors (see e.g. [26]) who stress out a dependence of the linear momentum transfer on the projectile velocity, or more precise, the relative velocity above the fusion barrier.

For $A_{res} > 200$ we observe a significant dependence of the mean velocity on both the residue masses and the masses of the compound nuclei. While the mass dependence of the mean velocity for a fixed compound nucleus reflects the influence of the preequilibrium emission on the mass of the residues (see sect. 5.1), the dependence on the masses of the compound nuclei reflects the high fission competition, due to which preequilibrium emission enhances the survival probability.

From this side differences in the mean velocities are somewhat 'artificial' and do not directly reflect the mean momentum transfer in the nuclear reaction, since the velocity distribution of the evaporation residues is further influenced by the deexcitation process. This is also visible for the reactions using different projectiles. The residues from $^{40}\text{Ar} + ^{181}\text{Ta} \rightarrow ^{221}\text{Pa}$ ($E^* = 371$ MeV), full triangles) appear to have higher mean velocities than those from $^{20}\text{Ne} + ^{197}\text{Au} \rightarrow ^{217}\text{Ac}$ ($E^* = 227$ MeV), although the masses of the compound nuclei are similar, while the excitation energies are significantly different. So the residue velocity is not only determined by the probability and multiplicity for preequilibrium emission but also from the number of thermal particles emitted before fission can compete with particles emission, because the mass and the atomic number of this intermediate nucleus will determine essentially the fission to evaporation ratio. By this measured velocity distributions of residues reflect processes leading to their production, but are less suited to draw 'global' conclusions on general aspects of complete or incomplete fusion.

5.4 Preequilibrium α - particles

The intensities of the preequilibrium α - particles observed in our experiment are shown in fig. 10 (full dots) as a function of the projectile energy and are compared with the results of Fuchs et al. [22] (open circles). Normalising our data at $E_p = 298$ MeV, to the result of [22] at $E_p = 290$ MeV, we find good agreement also at $E_p = 228$ MeV with the value reported in [22] at $E_p = 220$ MeV. At the lower energies our data are principally in-line with a 'smooth' trend from the values at higher energies (full line). This trend does not indicate a threshold energy for preequilibrium emission, but the steep decrease towards the lowest energies rather seem to be connected with the sharp drop of the fusion cross section when the fusion barrier ($E_B = 101.7$ MeV [27]) is reached.

6. Conclusion

Velocity and mass distributions of residues from bombardments of ^{197}Au and ^{165}Ho with ^{20}Ne at $E = 298$ MeV have been investigated. It has been shown, that the residue production is predominantly accompanied by emission of preequilibrium particles, which results in mean velocities of the residues significantly lower than v_{CN} . Comparisons of the mass distributions of astatine and polonium isotopes from the irradiations of ^{197}Au with results from evaporation codes indicate a shift of the experimental distributions to higher mass values compared to the model calculations. The latter also indicate, that this shift can also not be explained by fusion after projectile break-up according to the sum-rule model as it can at lower energies, so we tentatively assign it to preequilibrium emission from the interaction zone at the beginning of equilibration. But we have to note, that the production rates appear essentially higher for the heaviest residues than the prediction of the standard hybrid model. As those nuclei exhibit the lowest mean velocities, it seems likely that the emission rate of preequilibrium α particles is underpredicted. We also measured light particle (protons, α particles, Li- and Be- nuclei) energy spectra. A more detailed analysis of the α particle - spectra was performed. Two components, one ascribed to 'thermal - evaporation' particles and one, having same velocities as the projectiles to 'preequilibrium' particles. The intensity of the latter drops drastically towards lower bombarding energy, but there seems real threshold energy for preequilibrium α - particle emission, it rather seems to vanish at $E_{lab} \approx 100$ MeV ($E^* \approx 45$ MeV) i.e. at energies around the fusion barrier.

Acknowledgement

The experiment was performed in collaboration with A. Lüttgen (deceased) and V. Ninov in June, 1991. The author thanks A. Sitarcik for providing an updated version of fig. 5.

REFERENCES

- [1] K. Siwek-Wilczynska, E.H. du Marchie van Voorthuysen, J. van Popta, R.H. Siemssen, J. Wilczynski, Nucl. Phys. **A330**, 150 (1979).
- [2] J. Wilczynski, K. Siwek-Wilczynski, J. van Driel, S. Gongrijb, D.C.J.M. Hageman, R.V. Janssens, J. Lukasiak, R.H. Siemssen, S.Y. van der Werf, Nucl. Phys. **A373**, 109 (1982).
- [3] M. Blann, Phys. Rev. **C23**, 205 (1981).
- [4] M. Blann, Phys. Rev. **C31**, 1245 (1985).
- [5] F.P. Heßberger, V. Ninov, U. Spoerel, Z. Phys. **A340**, 171 (1991).
- [6] F.P. Heßberger, V. Ninov, S. Hofmann, D. Ackermann, S. Saro, M. Veselsky, Proc. 'International School Seminar on Heavy Ion Physics', Dubna, Russia, May 10-15, 1993; eds. Yu.Ts. Oganessian, Yu.E. Peionzhkevich, R. Kalpachieva, Vol.2, 3 (1993)
- [7] F.P. Heßberger, V. Ninov, S. Hofmann, D. Ackermann, S. Saro, M. Veselsky, Z. Phys. **A348**, 301 (1994).
- [8] M. Veselsky, S. Saro, F.P. Heßberger, V. Ninov, S. Hofmann, D. Ackermann, Z. Phys. **A356**, 403 (1998).
- [9] G. Münzenberg, W. Faust, S. Hofmann, P. Armbruster, K. Güttner, H. Ewald, Nucl. Instr. Meth. **161**, 65 (1979).
- [10] W. Faust, G. Münzenberg, S. Hofmann, W. Reisdorf, K.-H. Schmidt, P. Armbruster, Nucl. Instr. Meth. **166**, 397 (1979).
- [11] W. Reisdorf, F.P. Heßberger, K.D. Hildenbrand, S. Hofmann, G. Münzenberg, K.-H. Schmidt, J.R.H. Schneider, W.F.W. Schneider, K. Sümmerer, G. Wirth, J.V. Kratz, G. Schlitt, Nucl. Phys. **A438**, 212 (1985).
- [12] F.P. Heßberger, G. Münzenberg, P. Armbruster, G. Berthes, W. Faust, S. Hofmann, W. Reisdorf, K.-H. Schmidt, H. Ewald, K. Güttner. Proc. Symposium 'Heavy Ion Interactions around the Coulomb Barrier', Legnaro, Italy, June 1-4, 1988, Lecture Notes in Physics 317, eds. C. Signorini, S. Skorka, P. Spolaore, A. Vitturi, Springer Verlag, Berlin. Heidelberg, New York, London, Paris, Tokyo, 289 (1988).
- [13] F.P. Heßberger, GSI-Report GSI-85-11 (1985)
- [14] H. Essel, M. Richter, H. Grein, H. Sohlbach, W. Spreng, GOOSY Manuals, GSI 1988 (unpublished).
- [15] H. Göringer, S. Gralla, P. Malzacher, M. Richter, D. Schall, K. Winkelmann, GSI Report 88-16 (1988).
- [16] B. Cramer, thesis, Freie Universität Berlin (1989).
- [17] W. Reisdorf, Z. Phys.
- [18] M. Blann, J. Bisplinghoff, Report UCID - 19614 (1982).
- [19] L.C. Northcliffe, R.F. Shilling, Nucl. Data Tables **A7**, 233 (1970).
- [20] F. Hubert, R. Bimbot, H. Gauvin, Atomic Data and Nucl. Data Tables **A46**, 1 (1990).
- [21] L.E. Tubbs, J.R. Birkelund, J.R. Huizenga, D. Hilscher, U. Jahnke, H. Rossner, B. Gebauer, Phys. Rev. **C32**, 214 (1985).
- [22] H. Fuchs, M. Bürgel, H. Homeyer, G. Ingold, U. Jahnke, G. Thoma, Phys. Rev. **C31**, 465 (1985).
- [23] D. Hilscher, H. Rossner, Ann. Phys. Fr. **17**, 471 (1992).
- [24] K. Krishan, S. Bhattacharya, J.N. De, S.K. Samaddar, Nucl. Phys. **A543**, 159 (1992).
- [25] F.P. Heßberger, V. Ninov, D. Ackermann, A. Lüttgen, Nucl. Phys. **A568**, 121 (1994).
- [26] C. Gregoire, B. Tamain, Ann. Phys. Fr. **11**, 323 (1986).
- [27] R. Bass Nucl. Phys. A **231**, 45 (1974).